

MIT Open Access Articles

Chemical Expansion and Frozen-In Oxygen Vacancies in Pr-Doped Ceria

The MIT Faculty has made this article openly available. **Please share** how this access benefits you. Your story matters.

Citation: Kuru, Yener, Sean R. Bishop, Jae-Jin Kim, Bilge Yildiz, and Harry L. Tuller. "Chemical Expansion and Frozen-In Oxygen Vacancies in Pr-Doped Ceria." ECS Transactions 35:1 (2011). p. 1131-1136. © 2011 ECS - The Electrochemical Society.

As Published: <http://dx.doi.org/10.1149/1.3570094>

Publisher: Electrochemical Society

Persistent URL: <http://hdl.handle.net/1721.1/81873>

Version: Final published version: final published article, as it appeared in a journal, conference proceedings, or other formally published context

Terms of Use: Article is made available in accordance with the publisher's policy and may be subject to US copyright law. Please refer to the publisher's site for terms of use.





the society for solid-state
and electrochemical
science and technology

Journal of The Electrochemical Society

Anomalous Chemical Expansion Behavior of $\text{Pr}_{0.2}\text{Ce}_{0.8}\text{O}_{2-\delta}$ Thin Films Grown by Pulsed Laser Deposition

Y. Kuru, D. Marrocchelli, S. R. Bishop, D. Chen, B. Yildiz and H. L. Tuller

J. Electrochem. Soc. 2012, Volume 159, Issue 11, Pages F799-F803.
doi: 10.1149/2.016212jes

Email alerting service

Receive free email alerts when new articles cite this article - sign up
in the box at the top right corner of the article or [click here](#)

To subscribe to *Journal of The Electrochemical Society* go to:
<http://jes.ecsdl.org/subscriptions>



Anomalous Chemical Expansion Behavior of $\text{Pr}_{0.2}\text{Ce}_{0.8}\text{O}_{2-\delta}$ Thin Films Grown by Pulsed Laser Deposition

Y. Kuru,^{a,b,c,z} D. Marrocchelli,^{b,d,z} S. R. Bishop,^{a,e,*} D. Chen,^a B. Yildiz,^b and H. L. Tuller^{a,*}

^aDepartment of Materials Science & Engineering, Massachusetts Institute of Technology, Cambridge, Massachusetts 02139, USA

^bDepartment of Nuclear Science & Engineering, Massachusetts Institute of Technology, Cambridge, Massachusetts 02139, USA

^cDepartment of Materials Science & Engineering, Akdeniz University, Dumlupinar Bulvari Kampus, Antalya 07058, Turkey

^dSchool of Chemistry, Trinity College Dublin, College Green, Dublin 2, Ireland

^eInternational Institute for Carbon Neutral Energy Research (WPI-I2CNER), Kyushu University, Nishi-ku Fukuoka 819-0395, Japan

The chemomechanical and electrical properties of $(\text{Pr,Ce})\text{O}_{2-\delta}$ thin films were studied between 30 and 875°C in air by in situ X-ray diffraction and complex impedance spectroscopy measurements. Reduction/oxidation reactions produced large stress variations (~2 GPa) in the structure. Atomistic simulation techniques were employed to investigate the mechanisms behind the observed chemical expansion behavior, suggesting the possible roles of defect ordering upon cooling and heating. An alternative explanation based on a metastable frozen in state of higher reduction is also considered. Similar phenomena, observed here in $\text{Pr}_{0.2}\text{Ce}_{0.8}\text{O}_{2-\delta}$, are expected to be applicable and of potential significance for other technologically important complex oxides such as perovskite-structured materials.

© 2012 The Electrochemical Society. [DOI: 10.1149/2.016212jes] All rights reserved.

Manuscript submitted July 26, 2012; revised manuscript received August 30, 2012. Published September 24, 2012.

Non-stoichiometric oxides exhibit characteristics that are useful for their application in sensors,¹ oxygen storage in three way catalysts^{2,3} and solid oxide fuel cells (SOFC),^{4–7} due to their ability to change oxygen content with changes in environmental conditions and their mixed ionic electronic conductivity. The rate of oxidation/reduction of these materials is typically increased by moving to smaller dimensions, e.g. thin films or nanosized particles, leading to more rapid sensor response, more efficient catalysis, and lower SOFC resistance.^{8,9} Upon changes in temperature and partial pressure of oxygen, $p\text{O}_2$, the concentration of oxygen vacancies and other point defects in these materials changes, resulting not only in changes in electrical properties, but also in defect-induced changes in lattice parameter, known as chemical expansion,^{10–13} arising from the corresponding change in cation radii and oxygen vacancy formation/annihilation.¹⁴ In thin films, residual stresses and stress gradients can develop due to chemical expansion, as well as other sources such as thermal expansion mismatch between film and substrate, growth stresses and microstructural stabilization,^{15–18} potentially resulting in decreased structural stability of thin film devices. Lattice strain values, for example in $\text{Ce}_{0.8}\text{Gd}_{0.2}\text{O}_{1.9-\delta}$ thin films, reportedly vary between 0 and 7% depending on the film processing route and degree of crystallinity.¹⁹ Lubomirsky and co-workers report that strained free standing ceria thin film membranes exhibit changes in oxygen vacancy ordering.²⁰ Oxygen vacancy ordering is also deduced based on neutron diffraction experiments and reverse Monte Carlo modeling on bulk $\text{CeO}_{2-\delta}$,²¹ $\text{Ce}_{1-x}\text{Y}_x\text{O}_{2-x/2}$,²² and on several doped zirconia systems.^{23–25}

In literature, there are numerous investigations focused on phase equilibria and reduction/oxidation behavior of $\text{Pr}_x\text{Ce}_{1-x}\text{O}_{2-\delta}$ system. For instance, phase equilibria in $\text{PrO}_{2-\delta}$ was studied in Refs. 26 and 27 and stability fields of different phases were determined. McCullough produced $\text{Pr}_x\text{Ce}_{1-x}\text{O}_{2-\delta}$ solid solutions, heat treated in vacuum, air and oxygen, and reported the lattice parameters of the obtained fluorite phases. According to the results, single phase $\text{Pr}_x\text{Ce}_{1-x}\text{O}_{2-\delta}$ solid solutions can be synthesized in the entire composition range if the heat treatments are performed in air or under high O_2 pressure.²⁸ Zhou and Gorte studied phase stability and redox properties of $\text{Pr}_{0.2}\text{Ce}_{0.8}\text{O}_{2-\delta}$ and $\text{Pr}_{0.5}\text{Ce}_{0.5}\text{O}_{2-\delta}$ solid solutions.²⁹ They concluded that the observed reduction properties are close to the expected behavior of the physical mixtures of pure oxides; the enhanced reduction observed for the

solid solutions compared to pure CeO_2 stems from the fact that O can be easily removed from praseodymia compared to ceria.²⁹ Moreover, $\text{Pr}_x\text{Ce}_{1-x}\text{O}_{2-\delta}$ solid solutions were produced and their reduction tendency was compared to $\text{Zr}_x\text{Ce}_{1-x}\text{O}_2$ and $\text{Pr}_x\text{Zr}_{1-x}\text{O}_{2-\delta}$ systems in Ref. 30. Logan and Shelef investigated desorption, reduction and oxidation behavior for $\text{Pr}_x\text{Ce}_{1-x}\text{O}_{2-\delta}$ system and influence of noble metals (e.g. Pd) on these processes.³¹ It was reported that the reduction process is promoted in $\text{Pr}_{0.55}\text{Ce}_{0.45}\text{O}_{2-\delta}$ and Pr_6O_{11} by addition of Pd.³¹ Similarly, Chun et al. carried out reduction experiments for Pd catalyzed $\text{Pr}_x\text{Ce}_{1-x}\text{O}_{2-\delta}$ and concluded that the average temperature and the degree of reduction can be controlled by adjusting the Pr/Ce ratio.³²

In the present study, we investigated, by in-situ X-ray diffraction (XRD) measurements, the variation of strain-free lattice parameter and residual stress in $\text{Pr}_{0.2}\text{Ce}_{0.8}\text{O}_{2-\delta}$ (PCO) thin films, deposited onto (111) 8 mol% Y_2O_3 doped ZrO_2 (YSZ) substrates and highlighted the connection between the widely studied redox properties of the system and the resulting stress build up in thin film structures for the first time. An anomalous expansion starting at ~325°C was observed only upon the initial heating of as-prepared films. Additionally, an anomaly in electrical conductivity measurements (on a $\text{Pr}_{0.1}\text{Ce}_{0.9}\text{O}_{2-\delta}$ thin film) was also observed during the initial heating in the same temperature range. Further heating/cooling cycles resulted in reversible conductivity and expansion behavior. Atomistic simulations are used to probe the origin of the anomalous behavior. Similar phenomena observed here in PCO, are expected to be applicable and of potential significance for other technologically important complex oxides such as perovskite-structured materials.³³

Experimental

For XRD, a PCO thin film (nominal thickness ~490 nm) was deposited onto a (111) YSZ single crystal substrate by pulsed laser deposition (PLD) using a KrF excimer laser, emitting at 248 nm, as discussed in prior work.³⁴ The energy per pulse, repetition rate and target to substrate distance were 400 mJ/pulse, 8 Hz and 8 cm, respectively. After reaching a background pressure of less than 9×10^{-6} Torr, the film was deposited at 725°C under 10 mTorr O_2 pressure. Thereafter, the PCO thin film was cooled to room temperature under an O_2 pressure of 6–7 Torr, to aid in oxidation of the film.

The 2θ - ω scans (2θ is the angle between the incident and the diffracted X-ray beams; ω is the angle between the incident beam and the specimen surface) were carried out by a high resolution four-circle Bruker D8 Discover diffractometer, equipped with a Göbel mirror,

*Electrochemical Society Active Member.

^zE-mail: ykuru@mit.edu; D.Marrocchelli@tcd.ie

Eulerian cradle, 3-bounce Ge 022 analyzer crystal and a scintillation counter, using Cu $K\alpha_1$ radiation. The parallel beam condition, useful for elimination of various error sources such as sample displacement error, flat specimen error and sample transparency error, was satisfied by use of the combination of Göbel mirror and the analyzer crystal. An Anton Paar DHS 900 heating stage, capable of heating the specimen from room temperature to 900°C, was mounted to the sample stage during in-situ measurements under ambient pressure.

The interplanar spacing of (111) planes was measured at two inclination angles, ψ , (i.e. the angle between the diffraction vector and the specimen surface normal), 0 and 70.5°. The residual stresses (σ_{\parallel}) and strain-free lattice parameters (a_0) were obtained by crystallite group method since the PCO films are epitaxial.^{35,36} It is noted that the single-crystal elastic constants in Ref. 37 for CeO₂ were employed in this study to calculate the strain-free direction and σ_{\parallel} . The specimen was heated from 30°C to 875°C and cooled back to 30°C (i.e. so-called a heating/cooling cycle) two times, consecutively. The first heating and the final cooling steps were 45°C (i.e. between 30°C and 75°C); all the remaining temperature steps were 50°C upon both heating and cooling.

Electrical conductivity measurements were performed using a Novocontrol Alpha-A impedance analyzer with an AC amplitude of 50–300 mV and frequency range of 0.1 Hz to 1 MHz. Due to issues of film cracking when Pr_{0.2}Ce_{0.8}O_{2-δ} was deposited by PLD on electrically insulating sapphire substrates, Pr_{0.1}Ce_{0.9}O_{2-δ} thin films were used instead for electrical measurements. Au interdigitated electrodes with 100 μm spacing were deposited on the film surface by sputtering a pattern defined by photolithography, thereby obtaining a film resistance on the order of 0.1 GΩ at room temperature.

In this work a combination of Density Functional Theory calculations, within the DFT+U framework, and potential-based molecular dynamics simulations, was used. The interaction potential used for the molecular dynamics simulations is known as the DIPole Polarizable Ion Model (DIPPI) and includes a pair potential (a Buckingham term plus Coulombic interactions), together with an account of the polarization effects that result from the induction of dipoles on the ions. The parameterization and testing of this model were reported in a previous publication.³⁸ The accuracy of this model was found to be similar to that of DFT calculations, and the lower computational cost allows the performance of longer simulations on bigger systems. The lattice parameters for the studied systems were obtained by performing molecular dynamics simulations with 3 × 3 × 3 supercells in an NPT ensemble, at the required temperatures. Barostats and thermostats were used as described by Martyna et al.³⁹ and the external pressure was set to zero. The lattice parameters were typically averaged over long trajectories (~0.1 ns).

The Density Functional Theory calculations were performed with the Vienna Ab-initio Simulation Package (VASP),^{40,41} with the Projector Augmented Wave (PAW) method. The Generalized Gradient Approximation (GGA) with the Perdew-Wang 91 (PW91) exchange-correlation functional and an energy cutoff of 400 eV were employed. A Hubbard term was also added, U = 5 eV, to properly describe the localized nature of the Ce³⁺ *f* electrons. The slab method was used to simulate surfaces (160 atoms). All the calculations were carried out using the Brillouin zone sampled with a (3 × 3 × 1) Monkhorst-Pack mesh *k*-points grid. These settings are in line with those previously used in the literature⁴² and convergence tests were performed to make sure that the results are well converged with respect to these parameters.

Results and Discussion

Figure 1 demonstrates that the 490 nm thick PCO thin films grew epitaxially on the (111) YSZ substrates. Only {111} planes of the film are parallel to the substrate surface (cf. Figure 1a) and there are three peaks at $\psi = 54.7^\circ$ in the 200 pole figure of the PCO film, consistent with the angle between the (111) and (200) planes (cf. Figure 1b).

Figure 2 shows the evolution of the strain-free lattice parameter, a_0 , for PCO as a function of temperature during two consecutive heat-

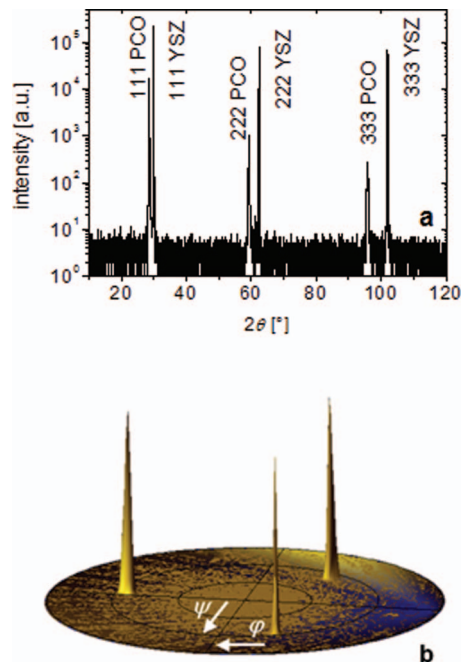
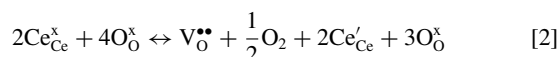
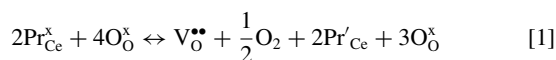


Figure 1. (a) The 2θ-ω scan and (b) the 200 pole figure of the PCO film on (111) YSZ substrate.

ing/cooling cycles. An increase of a_0 with increasing temperature, T , is observed. For this class of materials, this is usually due to two sources: (i) pure thermal expansion of the unit cell caused by the asymmetry of the potential energy curve,^{38,43} and (ii) chemical expansion of the unit cell due to oxygen loss from the lattice,^{12–14} according to Reactions 1 and/or 2, written in the Kröger-Vink notation⁴⁴



In PCO, chemical expansion arises upon the reduction of Pr⁴⁺ and/or Ce⁴⁺ cations to their respective 3+ valence states.^{10–13} The equilibrium equation for Reaction 1 is given by

$$\frac{[\text{Pr}_{\text{Ce}}']^2 [\text{V}_{\text{O}}^{\bullet\bullet}] p_{\text{O}_2}^{1/2}}{[\text{Pr}_{\text{Ce}}^{\times}]^2 [\text{O}_{\text{O}}^{\times}]} = K_o \exp\left(-\frac{H_r}{kT}\right) \quad [3]$$

where terms in brackets represent concentrations, K_o is a constant, k is the Boltzmann constant, T is temperature, and H_r is the enthalpy for reduction. A similar equation can be written for Reaction 2. Due to a lower H_r for Reaction 1 (~1.9 eV), Pr⁴⁺ reduces to Pr³⁺ at lower temperatures and higher p_{O_2} (e.g. air) as compared to Reaction 2

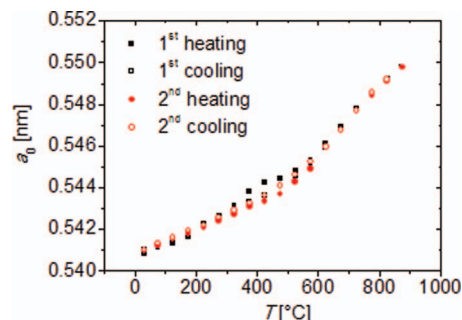


Figure 2. The strain-free lattice parameter, a_0 , versus temperature, T .

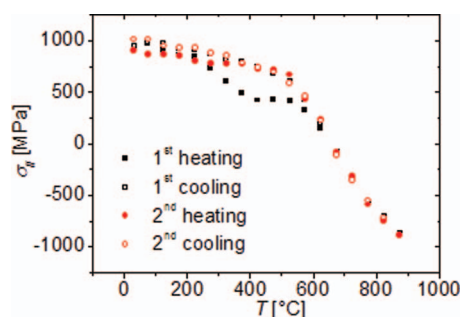


Figure 3. The residual stress, $\sigma_{//}$, versus temperature, T .

($H_r \sim 4.8$ eV) for Ce^{4+} reduction.^{12,45,46} Therefore, within the temperature range and pO_2 (air) of our experiments, 30–875°C, bulk chemical expansion arises entirely from the reduction of the Pr^{4+} cations and formation of oxygen vacancies,¹² in addition to possible oxygen vacancy ordering processes, discussed later.

Upon the 1st heating cycle shown in Figure 2, the strain-free lattice parameter, a_0 , increases linearly with T up to 325°C; then, a slight bump in a_0 is observed in the temperature range between 325 and 575°C and, finally, above 575°C, the curve resumes an approximately linear trend with steeper slope. The 1st cooling curve (open squares) overlaps with the 1st heating curve (closed squares), except for the temperatures between 325 and 575°C, corresponding to the *bump* feature (cf. Figure 2). Afterwards, a 2nd heating/cooling cycle is performed (corresponding to closed and open circles in Figure 2, respectively) with a_0 values following the same trend observed during the 1st cooling segment of the 1st heating/cooling cycle. The repeatable a_0 curves are nearly identical to the data reported for stress-free, nanocrystalline powders, heat treated under air, as described in Ref. 12.

In view of our previous results,^{12,13} the approximately linear behaviors of a_0 in the 30–325°C and 575–875°C temperature ranges can be ascribed to thermal expansion and thermal plus chemical expansion of the PCO thin film, respectively. However, the origin of the observed bump in a_0 , between 325 and 575°C, is not clear. Understanding the origin of variations in the lattice parameter of thin films is of great importance, since such variations might lead to large stresses in the film lattice and therefore to mechanical failure of the devices in which this material is used. For instance, the variation of residual stresses in the PCO film with temperature is reported in Figure 3. While $\sigma_{//}$ at 30°C is approximately 1 GPa tensile, it is released upon heating to ~650°C and, then, increases up to 1 GPa in the compressive direction at 875°C. Such high stress levels, especially at elevated temperatures, may create strong driving forces for mass transport processes and affect the mechanical stability of the PCO thin film.

In order to better understand whether the anomalous bump is related to a change in defect concentration and/or mobility, electrical conductivity measurements were performed on similar thin films. In Figure 4, the conductivity increases with temperature, but at 420–480°C, the rate of increase is reduced, and above this temperature range, it increases again, leading to the indicated *bump*. Further cooling and heating cycles do not show this anomalous feature. When heating in air, the electrical conductivity of PCO is proportional to the concentration of electronic and ionic defects as well as their thermally activated mobilities,⁴⁷ therefore, conductivity may increase in the bump region upon heating from 1) a decreased reduction enthalpy (see equation 3) of the post-deposition metastable structure as compared to the annealed material, leading to a higher concentration of conducting defects, 2) a higher concentration of defects frozen-in to room temperature from the highly energetic deposition conditions and subsequently annealed out, and/or 3) an order/disorder of frozen-in defects, affecting both concentration and mobility of defects, discussed below.

At the relatively low temperatures of the present measurements, together with the high concentration of oxygen vacancies which may be frozen-in during film fabrication, defect ordering can be expected.²¹

Table I. Lattice parameters for the DCO and OCO systems and relative contraction caused by O vacancy ordering. These values were determined by potential-based molecular dynamics simulations.

$[\text{V}_{\text{O}}^{\bullet\bullet}]$	Lattice Parameter OCO	Lattice Parameter DCO	Lattice Contraction [%]
1%	5.4298	5.4315	0.032
1.5%	5.4323	5.4351	0.050
2%	5.4359	5.4390	0.056

Furthermore, given the previously suggested relationship between oxygen vacancy ordering and chemical expansion,^{47,48} the effect of oxygen vacancy ordering/disordering on lattice parameter was therefore investigated using atomistic simulations. Since defect ordering tendencies are usually driven by electrostatic and steric effects,²⁵ expected to be similar for reduced Ce and Pr (both elements having the same valence states (4+ and 3+) and nearly identical ionic radii⁴⁹), simulations were performed on pure ceria (i.e. no Pr dopant). Two $\text{CeO}_{2-\delta}$ systems were studied, one with randomly distributed O vacancies and Ce^{3+} , with ions allowed to relax locally (i.e. no diffusion) at 100 K (termed disordered ceria, DCO). The second system was obtained by annealing the DCO system at high temperature (~2000 K), followed by slow cooling to 100 K. Due to the higher temperatures and slow cooling, O vacancies diffused, resulting in an ordered phase referred to as ordered $\text{CeO}_{2-\delta}$ (OCO). In OCO, the O vacancies tend to be nearest neighbor to Ce^{4+} , next nearest neighbor to Ce^{3+} and preferentially order with respect to each other along the (111) directions, consistent with the reports on similar systems.^{22–24} As shown in Table I, the lattice parameter for OCO is consistently smaller than DCO, meaning that O vacancy ordering leads to a contraction of the lattice parameter, in agreement with prior investigations.⁴⁷

The results obtained from experiments and atomistic simulations can be combined to provide a possible explanation for the anomalous bump observed in Figures 2 and 4. Turning back to scenario 3), a large concentration of disordered, frozen-in defects may have formed upon the highly energetic PLD film fabrication which were not sufficiently annealed out during the mild post-processing treatment. Upon heating (and thus overcoming kinetic limitations), the defects are believed to begin to order above 450°C, consequently resulting in a decrease in the rate of expansion. Additionally, upon heating in this region, the film will oxidize, thus removing frozen-in defects as well as contributing to a reduced expansion rate. Finally, the annealing away of frozen-in defects results in the observed reversibility with further heating/cooling cycles.

The above case does not, however, explain the initial lower temperature onset of the increase in lattice parameter (chemical expansion) versus the later thermal cycles. As an alternative explanation, scenario 1), the post-deposited material exhibits a meta-stability with enhanced

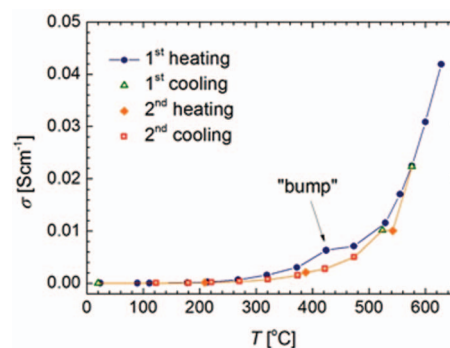


Figure 4. Electrical conductivity upon two heat/cool cycles of a 117 nm thick $\text{Pr}_{0.1}\text{Ce}_{0.9}\text{O}_{2-\delta}$ film deposited on a (0001) oriented Al_2O_3 substrate. A “bump” in conductivity is observed upon the first heat at the same temperature range as that observed in strain-free lattice parameter and stress data (Figs. 2 and 3).

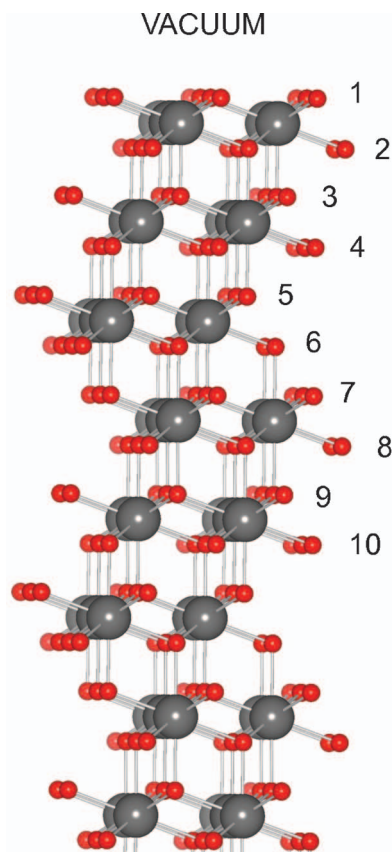


Figure 5. Snapshot of the ceria slab used to evaluate the vacancy formation energy for vacancies at different layers of the slab.

reducibility (decreased H_r in equation 3), leading to an increase in oxygen vacancy concentration at lower temperatures upon heating, with consequent chemical expansion and increased conductivity, as compared to the stable, reversible case. Like before, upon heating to higher temperatures, the metastability is annealed away, leading to the observed reversible behavior upon later thermal cycling.

A potential source of apparent enhanced reducibility is a large fraction of interfaces, which due to their low crystallinity are known to be more reducible than the bulk.⁸ To investigate this source, a simulation was used to obtain information about the influence of crystallite size (proportional to interface/bulk fraction) on O vacancy concentration (see Figure 5 for a snapshot of the ceria slab used to evaluate the vacancy formation energy for vacancies at different layers of the slab). In Table II, it is clear that energies required for defect

formation are decreased near the $\text{CeO}_2(111)$ surface, with values away from the surface converging to the bulk value. However, in HTXRD measurements on PCO powders (also exhibiting the above anomalous lattice parameter behavior), crystallite size was not observed to change in the region where the anomalous expansion occurs.⁵⁰ Therefore, the metastability may stem from another source, under investigation.

Conclusions

As demonstrated, thin films of non-stoichiometric complex oxides are prone to large volume changes when they are in contact with oxidizing and/or reducing atmospheres. These volume changes, accompanied by the development of residual stresses in the structure due to clamping of the film to the rigid substrate, may severely affect the mechanical stability of the thin film. Therefore, these volume variations must be well understood in order to guarantee a long life for the components produced from these materials. In this study, the thermo-chemical expansion and associated residual stresses and electrical conductivity in PCO thin films were measured by in-situ X-ray diffraction and impedance spectroscopy measurements, respectively. An anomalous *bump* was observed both in the lattice expansion and electrical conductivity versus temperature curves. Atomistic simulation techniques were employed to investigate the mechanisms behind the observed anomalous chemical expansion behavior, suggesting the possible roles of defect ordering/upon cooling and heating. An alternative explanation based on a metastably frozen in state of higher reduction was also considered. Irrespective of the source of these anomalies, reduction/oxidation reactions were observed to produce large stress variations (~ 2 GPa) in the structure, with potential for major impact on properties or film fracture. Similar phenomena, observed here in PCO, are expected to be applicable and of potential significance for other technologically important complex oxides such as perovskite-structured materials.

Acknowledgments

This research is being funded by the MIT Energy Initiative Seed Fund Program and the Basic Energy Sciences, Department of Energy under award DE SC0002633. SRB recognizes support from I2CNER, supported by the World Premier International Research Center Initiative (WPI), MEXT, Japan. DM wishes to thank the Government of Ireland for an EMPOWER Postdoctoral Fellowship. Y. Kuru and D. Marrocchelli equally contributed to this paper.

References

1. P. G. Bruce, *Solid State Electrochemistry*, Cambridge University Press, Cambridge (1995).
2. A. Tschöpe, W. Liu, M. Flytzani-Stephanopoulos, and J. Y. Ying, *J. Catal.*, **157**, 42 (1995).
3. A. Trovarelli, *Catal. Rev. Sci. Eng.*, **38**, 439 (1996).
4. A. Atkinson, *Solid State Ionics*, **95**, 249 (1997).
5. H. L. Tuller, *Solid State Ionics*, **52**, 135 (1992).
6. B. C. H. Steele and A. Heinzel, *Nature*, **414**, 345 (2001).
7. A. J. Jacobson, *Chem. Mater.*, **22**, 660 (2010).
8. H. L. Tuller, *Solid State Ionics*, **131**, 143 (2000).
9. A. Kossy, Y. Feldman, E. Wachtel, I. Lubomirsky, and J. Maier, *Adv. Funct. Mater.*, **17**, 2393 (2007).
10. C. Chatzichristodoulou, P. V. Hendriksen, and A. Hagen, *J. Electrochem. Soc.*, **157**, B299 (2010).
11. C. Chatzichristodoulou and P. V. Hendriksen, *J. Electrochem. Soc.*, **157**, B481 (2010).
12. Y. Kuru, S. R. Bishop, J. J. Kim, B. Yildiz, and H. L. Tuller, *Solid State Ionics*, **193**, 1 (2011).
13. S. R. Bishop, H. L. Tuller, Y. Kuru, and B. Yildiz, *J. Eur. Ceram. Soc.*, **31**, 2351 (2011).
14. D. Marrocchelli, S. R. Bishop, H. L. Tuller, and B. Yildiz, *Adv. Funct. Mater.*, **22**, 1958 (2012).
15. L. B. Freund and S. Suresh, *Thin Film Materials: Stress, Defect Formation and Surface Evolution*, Cambridge University Press, Cambridge (2003).
16. M. Ohring, *Materials Science of Thin Films*, Academic Press, San Diego (2002).
17. Y. Kuru, M. Wohlschlögel, U. Welzel, and E. J. Mittemeijer, *Thin Solid Films*, **516**, 7615 (2008).
18. Y. Kuru, M. Wohlschlögel, U. Welzel, and E. J. Mittemeijer, *J. Appl. Crystallogr.*, **41**, 428 (2008).

Table II. Vacancy formation energies for O vacancies from different distances from the surface. These values were calculated using DFT+U calculations.

Layer	E_{vac} [eV]
1	2.57
2	2.36
3	2.54
4	3.11
5	3.05
6	3.18
7	3.04
8	3.11
9	2.99
10	3.20
Bulk	3.06

19. J. L. M. Rupp, *Solid State Ionics*, **207**, 1 (2012).
20. A. Kossoy, Y. Feldman, R. Korobko, E. Wachtel, I. Lubomirsky, and J. Maier, *Adv. Func. Mater.*, **19**, 634 (2009).
21. S. Hull, S. T. Norberg, I. Ahmed, S. G. Eriksson, D. Marrocchelli, and P. A. Madden, *J. Solid State Chem.*, **182**, 2815 (2009).
22. M. Burbano, S. T. Norberg, S. Hull, S. G. Eriksson, D. Marrocchelli, P. A. Madden, and G. W. Watson, *Chem. Mater.*, **24**, 222 (2012).
23. S. T. Norberg, S. Hull, I. Ahmed, S. G. Eriksson, D. Marrocchelli, P. A. Madden, P. Li, and J. T. S. Irvine, *Chem. Mater.*, **23**, 1356 (2011).
24. D. Marrocchelli, P. A. Madden, S. T. Norberg, and S. Hull, *Chem. Mater.*, **23**, 1365 (2011).
25. D. Marrocchelli, P. A. Madden, S. T. Norberg, and S. Hull, *J. Phys.: Condens. Mat.*, **21**, 405403 (2009).
26. R. E. Ferguson, E. D. Guth, and L. Eyring, *J. Am. Chem. Soc.*, **76**, 3890 (1954).
27. B. G. Hyde, D. J. M. Bevan, and L. Eyring, *Philos. T. R. Soc. A*, **259**, 583 (1966).
28. J. D. McCullough, *J. Am. Chem. Soc.*, **72**, 1386 (1950).
29. G. Zhou and R. J. Gorte, *J. Phys. Chem. B*, **112**, 9869 (2008).
30. C. K. Narula, L. P. Haack, W. Chun, H. W. Jen, and G. W. Graham, *J. Phys. Chem. B*, **103**, 3634 (1999).
31. A. D. Logan and M. Shelef, *J. Mater. Res.*, **9**, 468 (1994).
32. W. Chun, G. W. Graham, J. A. Lupescu, R. W. McCabe, M. M. Koranne, and R. Brezny, *Catal. Lett.*, **106**, 95 (2006).
33. R. H. E. van Doorn and A. J. Burggraaf, *Solid State Ionics*, **128**, 65 (2000).
34. D. Chen, S. R. Bishop, and H. L. Tuller, *J. Electroceram.*, **28**, 62 (2012).
35. U. Welzel, J. Ligt, P. Lamparter, A. C. Vermeulen, and E. J. Mittemeijer, *J. Appl. Crystallogr.*, **38**, 1 (2005).
36. V. Hauk, *Structural and Residual Stress Analysis by Nondestructive Methods: Evaluation-Application-Assessment*, Elsevier, Amsterdam (1997).
37. V. Kanchana, G. Vaitheeswaran, A. Svane, and A. Delin, *J. Phys.: Condens. Mat.*, **18**, 9615 (2006).
38. M. Burbano, D. Marrocchelli, B. Yildiz, H. L. Tuller, S. T. Norberg, S. Hull, P. A. Madden, and G. W. Watson, *J. Phys.: Condens. Mat.*, **23**, 255402 (2011).
39. G. J. Martyna, D. Tobias, and M. L. Klein, *J. Chem. Phys.*, **101**, 4177 (1994).
40. G. Kresse and J. Hafner, *Phys. Rev. B*, **49**, 14251 (1994).
41. G. Kresse and J. Furthmuller, *Phys. Rev. B*, **54**, 11169 (1996).
42. D. Marrocchelli and B. Yildiz, *J. Phys. Chem. C*, **116**, 2411 (2012).
43. Y. Kuru, M. Wohlschlogel, U. Welzel, and E. J. Mittemeijer, *Appl. Phys. Lett.*, **90**, 243113 (2007).
44. Y.-M. Chiang, D. Birnie III, and W. D. Kingery, *Physical Ceramics: Principles for Ceramic Science and Engineering*, John Wiley & Sons Inc., New York (1997).
45. S. R. Bishop, T. S. Stefanik, and H. L. Tuller, *Phys. Chem. Chem. Phys.*, **13**, 10165 (2011).
46. S. R. Bishop, T. S. Stefanik, and H. L. Tuller, *J. Mater. Res.*, **27**, 2009 (2012).
47. S. R. Bishop, K. L. Duncan, and E. D. Wachsman, *Acta Mater.*, **57**, 3596 (2009).
48. A. Kossoy, J. P. Nair, E. Wachtel, I. Lubomirsky, J. Fleig, and J. Maier, *J. Electroceram.*, **13**, 605 (2004).
49. R. D. Shannon, *Acta Crystallogr. Sect. A*, **32**, 751 (1976).
50. Y. Kuru, D. Marrocchelli, S. R. Bishop, J. J. Kim, B. Yildiz, and H. L. Tuller, to be published.